

Trace Metal Bioremediation: Assessment of Model Components from Laboratory and Field Studies to Identify Critical Variables

Award ER62705-1011997-0003963

Peter Jaffe and Herschel Rabitz, PIs
John Houghton, Project Officer

Abstract

The objective of this project was to gain an insight into the modeling support needed for the understanding, design, and operation of trace metal/radionuclide bioremediation. To achieve this objective, a workshop was convened to discuss the elements such a model should contain. A “protomodel” was developed, based on the recommendations of the workshop, and was used to perform sensitivity analysis as well as some preliminary simulations in support for bioremediation test experiments at UMTRA sites.

To simulate the numerous biogeochemical processes that will occur during the bioremediation of uranium contaminated aquifers, a time-dependent one-dimensional reactive transport model has been developed. The model consists of a set of coupled, steady state mass balance equations, accounting for advection, diffusion, dispersion, and a kinetic formulation of the transformations affecting an organic substrate, electron acceptors, corresponding reduced species, and uranium. This set of equations is solved numerically, using a finite element scheme. The redox conditions of the domain are characterized by estimating the pE, based on the concentrations of the dominant terminal electron acceptor and its corresponding reduced specie. This pE and the concentrations of relevant species are passed to a modified version of MINTEQA2, which calculates the speciation and solubilities of the species of interest. Kinetics of abiotic reactions are described as being proportional to the difference between the actual and equilibrium concentration.

A global uncertainty assessment, determined by Random Sampling High Dimensional Model Representation (RS-HDMR), was performed to attain a phenomenological understanding of the origins of output variability and to suggest input parameter refinements as well as to provide guidance for field experiments to improve the quality of the model predictions. Results indicated that for the usually high nitrate contents found at many DOE sites, overall bioremediation of trace metals was highly sensitive to the formulation of the denitrification process.

Simulations were performed to illustrate the effect of biostimulation on the transport and precipitation of uranium in the subsurface, at conditions equivalent to UMTRA sites. These simulations predicted that uranium would precipitate in bands that are located relatively close to the acetate injection well. The simulations also showed the importance of properly determining U(IV) oxidative dissolution rates, in order to assess the stability of precipitates once oxygenated water reenters the aquifer after bioremediation is discontinued.

The objective of this project was to provide guidance to NABIR's Systems Integration Element, on the development of models to simulate the bioremediation of trace metals and radionuclides. Such models necessarily need to integrate hydrological, geochemical, and microbiological processes. In order to gain a better understanding of the key processes that such a model should contain, it was deemed desirable to convene a workshop with experts from these different fields. The goal was to obtain a preliminary consensus on the required level of detail for the formulations of these different chemical, physical, and microbiological processes. The workshop was held on December 18, 1998. A summary of the report [*Jaffé and Rabitz., 1998*] is given below.

I. WORKSHOP SUMMARY

Objectives

1. Identify the relevant biogeochemical issues and concepts necessary for NABIR models.
2. Start the process towards the identification of an effective long-term integrative modeling effort for the NABIR program.

Conclusions

The preliminary modeling effort should assume that the system has been driven anaerobic through the addition of an electron donor. This will be valuable to NABIR because it is anticipated that such a biostimulation experiment will be conducted at the Field Research Center. This will also simplify an already complex modeling task. The heterogeneity of organic carbon composition and distribution in natural environments, the long time scales in intrinsic bioremediation, the relative complexity of the biologic community in unstimulated conditions, and other factors make this a good place to start.

The preliminary modeling effort should be based on first principles rather than empirical data so that it will be more robust. It should focus on the major areas of NABIR investigator interest (i.e., denitrification, iron reduction, sulfate reduction, and perhaps fermentation). This modeling effort also will help identify areas for further modeling needs and research and help define the long-term integrative effort.

Many of the individual research projects already have specific modeling components directly integrated into them. The experience gained from these project-specific models will be valuable for the overall systems integration effort. The long-term integrative effort will evolve from the development of the preliminary effort and will need to complement the coordinated component studies.

The Systems Integration element will not work as a "modeling service". It might eventually link certain models from individual projects in some hierarchical framework, but individual projects should identify modeling resources to meet their own specific needs.

These recommendations are preliminary at this stage. The approach to the preliminary modeling effort will be refined in the coming months after a thorough review of the literature on modeling the biogeochemical dynamics of trace metals and

radioisotopes in the subsurface has been concluded. Further recommendations of members of the NABIR program are welcome.

Recommendations

Biogeochemical electron donor/acceptor processes

1. Description of redox transition zones. Two approaches to describe the transition between redox zones include: (a) Tracking of the electron acceptors, where the transition between redox zones is defined by the depletion of one electron acceptor and the rise of the next dominant one.
(b) Tracking of the partial pressure of hydrogen and the inclusion of a Monod-type formulation in the overall utilization rate of the electron acceptor that accounts for the hydrogen utilization biokinetic parameters for each bacterial population. Approach (b) was viewed as the more suitable, even though it requires simulation of hydrogen as an independent species. This clearly indicates that environmentally relevant fermentation processes could be critical, and more information in this area is needed.
2. Estimation of pE. The need to estimate pE as a master variable to drive geochemical equilibrium calculations was acknowledged. pE is conventionally estimated from the half reaction of the dominant electron acceptor. It was suggested that the potential of utilizing the hydrogen half cell be evaluated as an alternative.
3. Biotic and abiotic reactions. Both biotic and abiotic redox reactions need to be accounted for in viable models. Models should not be based on the assumption that chemical equilibrium conditions are reached during biostimulation. Kinetics of abiotic reactions may be conveniently expressed in terms of their degree of disequilibrium.

Bacterial dynamics

1. Biostimulation and bioaugmentation require very different types of modeling efforts, and should be modeled separately.
2. There is a need to simulate bacterial filtration and detachment during bioaugmentation. It appears necessary to go beyond simple colloid filtration models to evaluate the bacterial transport.
3. Bacterial activity was discussed as an overall important variable to describe bacterially mediated kinetic processes. Given the low bacterial activity and numbers in pristine subsurface environments, an accurate characterization of bacterial activity is currently difficult to formulate. Under conditions of excess carbon (such as might occur during bioremediation), it appears that the bacterial activity can be lumped into appropriate characteristic rate constants. This approach does not call for modeling of bacterial transport for simulating biostimulation dynamics.
4. Although there is agreement that, after biostimulation the bacterial population reverts to its original state, post closure bacterial dynamics are of public concern, and may need to be considered explicitly.

Time Scales

There is need for both short-term (e.g., a few years) and very long-term (e.g., decades) models. Long-term models need to account for processes such as weathering, intra-particle diffusion, and co-precipitation. There is also a need to understand and simulate the long-term stability of a microbially-based immobilization system.

Heterogeneities

Heterogeneities play a role in transport as well as directly influencing micro-environmental-scale chemical and biological processes. All aspects of biogeochemical processes need to consider multiscale heterogeneities. The full consequences of such heterogeneities are not completely understood at this time. Detailed modeling, laboratory, and field studies are needed to assess the regimes where heterogeneities play a significant role. The dispersion of data on different length scales and for different sites needs to be documented. The viability of simplified effective medium models needs to be explored.

Preliminary Modeling and Key Variable Identification.

- A. To gain an initial understanding of general model robustness and parameter interaction, a one-dimensional transient biogeochemical model (research-level tool) will be adapted to simulate the dynamics of uranium (and/or other trace metal species of interest) in groundwater under biostimulation.
- B. Given the importance of hydrogen for the subsurface microbiology, a formulation of hydrogen-based biogeochemical modeling will be developed for initial evaluation of its advantages, disadvantages, and knowledge gaps.
- C. Development of model analysis tools will proceed with specific emphasis on the treatment of biochemically significant broad variable ranges. Both random and ordered sampling capabilities will be pursued. Test cases will be performed on the model described in II.A., with the aim of providing an initial assessment of biogeochemical model robustness to physical/chemical/bacterial variables, and to allow for a more focused and goal-oriented planning of the near and intermediate-term modeling tasks to be conducted by the NABIR systems integration effort.

II. PRELIMINARY MODELING EFFORT APPLIED TOWARDS THE BIOREMEDIATION OF URANIUM-CONTAMINATED AQUIFERS

In response to the recommendations from the workshop, a preliminary model was developed and a rigorous model testing was performed on it in order to gain further insights into the robustness of a trace metal bioremediation model (Wang et al., 2002, highlights are given below).

Introduction

Mathematical models have been developed to simulate the biodegradation of organic substrates in groundwater systems. In these models, the biodegradation of organic substrates and the corresponding utilization of electron acceptors, as well as bacterial dynamics such as growth, decay, and transport have been incorporated into the advective-dispersive transport equations. Different chemical species have usually been simulated as either single or multiple limiting components [Borden and Bedient, 1986; Molz et al., 1986; Widdowson et al., 1988]. In recent years, models have been developed that included biologically mediated redox dynamics in terms of the sequential utilization of different electron acceptors during the degradation of an organic substrate [Rabouille and Gaillard, 1991; Sweerts et al., 1991; Matsunaga et al., 1993; McNab and Narasimhan, 1994; Van Cappellen and Wang, 1995; Dhakar and Burdige, 1996; Park and Jaffé, 1996]. Some of these models have been extended to include abiotic redox reactions and geochemical processes such as speciation and precipitation/dissolution [Wang and Van Cappellen, 1996; Hunter et al., 1998; Smith and Jaffé, 1998].

Based on these biological and geochemical processes, trace metals dynamics in groundwater have been described by several authors [e.g., Yeh and Tripathi, 1991; Engesgaard and Kipp, 1992; Lensing et al., 1994]. Although, in many of these studies, it was assumed that the metal is at equilibrium with the surrounding geochemistry, this is clearly not always the case. Non-equilibrium conditions have therefore been implemented in formulating the cycling of iron and manganese [i.e., McNab and Narasimhan, 1994; Hunter et al., 1998], and in the formulation of the dynamics of trace metals, where it has been assumed that the metals are driven kinetically towards chemical equilibrium [Smith and Jaffé, 1998].

Aqueous phase homogeneous reactions such as speciation, complexation, or acid-base reactions are usually described as instantaneous reactions. This is justified because their effect on the concentration of a chemical species is very fast compared to the change in concentration due to groundwater transport. These reactions are therefore represented in many models by thermodynamic equilibrium conditions [Grove and Wood, 1979; Miller and Benson, 1983; Narasimhan et al., 1986; Kirkner and Reeves, 1988; Reeves and Kirkner, 1988; Engesgaard and Kipp, 1992]. In contrast, biologically mediated reactions and heterogeneous reactions such as precipitation/dissolution are relatively slow and have been incorporated by several authors into transport models using kinetic relationships [Steeffel and Lasaga, 1994; Tebes-Stevens et al., 1998; VanBriesen and Rittmann, 1999].

In all areas of numerical modeling the issue of predictive quality, in view of model input uncertainty has been a topic of prime concern. Systematic uncertainty assessments can identify the inputs with the most influence and their behavior patterns on the model outputs. The resultant information can provide guidance for new experiments

or parameter estimations to reduce the output uncertainty. A general set of quantitative model assessment and analysis tools, termed High Dimensional Model Representation (HDMR), have been introduced recently for improving the efficiency of deducing high-dimensional input-output system behavior [Rabitz *et al.*, 1999; Alis *et al.*, 1999, 2000; Shorter *et al.*, 1999, 2000]. HDMR is an efficient approach for global uncertainty assessment of a model. With a modest sampling effort, HDMR can provide reliable information by decomposing the model output variance into its different input contributions such as the independent input variable action, the pair correlated action of inputs, etc. This information is most valuable for attaining a physical understanding of the origins of output uncertainty as well as suggestions for additional laboratory/field studies or parameter refinements to best improve the quality of model predictions.

The overall goal of a uranium bioremediation scheme is the stabilization of the uranium as U(IV)-minerals. The goal of this work was to identify the key parameter interactions and uncertainties in trace metal bioremediation models, specifically applied to the immobilization of uranium, in order to provide guidance for further model development and to link model development to ongoing fieldwork. To accomplish this goal, a “proto model” to simulate trace metal bioremediation was developed and applied to study the biological immobilization of uranium in groundwater. The HDMR method was then applied to this model to assess the relationship between the different model input parameters and model outputs.

A model designed to simulate trace-metal/radionuclide bioremediation in aquifers can include different levels of detail, in terms of the relevant geochemistry and bacterial dynamics, at varying scales. It was decided here to develop a model where the biomass is incorporated into the overall kinetic coefficients, rather than simulating bacterial growth, decay, and transport separately. The rationale for this decision was that: (1) successful field techniques for the *in situ* measurement of rate coefficients, such as the Push-Pull Test [Schroth *et al.*, 1998] yield bulk reaction rate coefficients that have the biomass incorporated; (2) during biostimulation, when a substantial amount of an easily degradable growth substrate is injected into the subsurface, one is likely to reach some maximum biomass level [Jaffé and Rabitz., 1998]; and (3) by not including complex bacterial dynamics, this already complex “proto model” does not require an additionally large number of parameters that are difficult to characterize, specially for field conditions.

The model consists of a set of coupled, time-dependent one-dimensional mass balance equations, which include physical processes such as advection, diffusion, and dispersion, and biogeochemical processes such as biotic and abiotic redox reactions, speciation, adsorption, and precipitation/dissolution of minerals, all of which can affect either the organic substrate, the terminal electron acceptors (oxygen, nitrate, Mn(IV), Fe(III), and sulfate), the corresponding reduced species, and the trace metals/radionuclides of interest. The system of mass balance equations is solved numerically, using a second-order-accurate finite difference scheme through a series of iterative routines. At each node and time step, the concentration profiles of chemical species are transferred to an equilibrium speciation model, which calculates the speciation and solubility of the species of interest.

The pH, along with other environmental variables such as temperature, is a key parameter that affects the fate of trace metals and other chemical constituents. The pH of

a groundwater system may vary spatially and with time. During biostimulation the different biotic and abiotic reactions may further affect the pH of the groundwater. For the purpose of this work, however, pH will not be calculated explicitly in the model but will be considered a model input. Dissolved-organic carbon-enhanced transport was not accounted for in the simulations shown here, but can be easily included by allowing for a partitioning of the relevant species between the dissolved organic carbon and the aqueous phase.

Model Development

The fate and transport of many trace metals and radionuclides in subsurface environments are closely linked to the biogeochemical reactions that occur as a result of the oxidation of organic carbon by different microorganisms using a series of terminal electron acceptors such as O_2 , NO_3^- , $Mn(IV)$, $Fe(III)$ and SO_4^{2-} . Throughout the redox profile that develops in such environments, various processes such as reduction/oxidation, sorption/desorption, precipitation/ dissolution, and/or the formation of complex ions can affect the fate of trace metals directly or indirectly. Therefore, to simulate the fate of trace metals/radionuclides in groundwater systems during biostimulation requires simultaneous consideration of biotic and abiotic reactions that affect the trace metals and/or radionuclides of interest.

Reactive Transport Equations

A system of one-dimensional mass balance equations was formulated for the dissolved and solid species of interest in a saturated porous medium:

$$\text{dissolved species: } \theta \frac{\partial C_i^{aq}}{\partial t} + D_{hi} \frac{\partial^2 C_i^{aq}}{\partial x^2} + v \frac{\partial C_i^{aq}}{\partial x} = R_i \quad (1)$$

$$\text{Solid species: } \frac{\partial C_j^s}{\partial t} = R_j \quad (2)$$

Where C_i^{aq} and C_j^s are the concentrations of the dissolved species i (in moles per unit volume of water) and the solid species j (in moles per unit volume of solid matrix) [M/V], respectively; v is the average linear velocity of groundwater flow [L/T]; D_{hi} is the hydrodynamic dispersion coefficient (mechanical dispersion + molecular diffusion) of dissolved species i [L²/T]; R_i and R_j are the net rates of consumption/production of the dissolved species i and the solid species j by geochemical and microbiological reactions (in moles per unit total volume of porous medium per unit time) [M/VT]; θ is the porosity [V/V]; and $K_{d,i}^{eff}$ is an effective partition coefficient for the equilibrium adsorption of species i , which is defined as the ratio of adsorbed to dissolved mass of specie i , calculated from MINTEQA2, per unit total volume of porous medium at each spatial node [M/M]. While dissolved species are transported via advection and dispersion, solid species are assumed stationary and their changes in concentrations are determined solely via biogeochemical reactions. The mass balance equations for each dissolved and solid species are coupled through the reaction terms, R_i and R_j , and form a system of partial and ordinary differential equations.

Biotic/Abiotic Redox Reaction Rate Expressions

During the degradation of organic substrates, some heterotrophic bacteria can utilize trace metals as a terminal electron acceptor, and thereby change the metal's physical and/or chemical characteristics. The kinetics of such microbial-mediated redox reactions has been expressed using various formulations that usually are a function of the concentrations of the electron donors and/or acceptors. Monod-type formulations have been widely used to describe the consumption/production rates of electron donors and acceptors in microbiological reactions [Widdowson *et al.*, 1988; Semprini and McCarty, 1992; McNab and Narasimhan, 1994; Salvage and Yeh, 1998; Smith and Jaffé, 1998]. Due to substantial amounts of external carbon sources supplied into the contaminated aquifer during biostimulation, and because high level of nitrate are common at many sites contaminated with uranium, the rate of biodegradation of the dissolved organic substrate can be formulated using a dual-Monod kinetics as:

$$R_C^{bio} = \frac{N_{eA} \cdot \frac{C_C}{K_{s,C} + C_C} \cdot \frac{C_{eA}}{K_{s,eA} + C_{eA}}}{\sum_{eA} \frac{C_C}{K_{s,C} + C_C} \cdot \frac{C_{eA}}{K_{s,eA} + C_{eA}}} \quad (3)$$

Where N_{eA} is the number of terminal electron acceptors considered; C_C and C_{eA} are the concentrations of the dissolved organic substrate and a given terminal electron acceptor [M/V]. α_{eA} is an indicator coefficient for the utilization of a terminal electron acceptor, which is determined by the concentration of the precedent terminal electron acceptor (in terms of energy yield). The indicator is equal to 1 when this electron acceptor is being utilized and equal to 0 when a more energetically favorable electron acceptor is still present at substantial concentration. Therefore, the utilization of a less energetically favorable terminal electron acceptor does not proceed until the concentration of the more favorable electron acceptor drops below a specified threshold level [Kindred and Celia, 1989; Rabouille and Gaillard, 1991; Kinzelbach *et al.*, 1991; Park and Jaffé, 1996]. $\mu_{m,eA}$ is the electron-acceptor-dependent rate of organic substrate oxidation [M/VT], which as discussed earlier includes the biomass in this formulation. $K_{s,eA}$ and $K_{s,C}$ are the half-saturation coefficients for the electron acceptor and the organic substrate [M/V], respectively. $K_{s,C}$ is assumed constant for all terminal electron acceptor pathways. The rate of consumption of a given terminal electron acceptor and the production of its corresponding reduced species are formulated as:

$$R_{eA}^{bio} = \frac{\alpha_{eA} \cdot \frac{C_C}{K_{s,C} + C_C} \cdot \frac{C_{eA}}{K_{s,eA} + C_{eA}}}{\sum_{eA} \frac{C_C}{K_{s,C} + C_C} \cdot \frac{C_{eA}}{K_{s,eA} + C_{eA}}} \quad (4)$$

$\alpha_{eA} R_{eA}^{bio}$ corresponding reduced species

Where α_{eA} is the stoichiometric coefficient representing the ratio of the number of moles of a given electron acceptor required to oxidize one mole of organic substrate [M/M]. Since the terminal electron acceptor in methanogenesis, CO_2 , was not explicitly simulated in this model, the rate of methanogenesis is formulated as a function of the organic substrate concentration only. The rate of oxidation of ammonia and the production of nitrate and the oxidation of methane as well as corresponding consumption of oxygen are also represented by a Monod-type expression.

The reduced species that are being produced in the process of the biodegradation of the organic substrate (i.e., Mn(II), Fe(II), and HS⁻), as well as NH₄⁺ and CH₄ can be re-oxidized when they are transported into a more oxidizing region. The rate of oxidation of dissolved reduced species i by dissolved oxidant j is formulated by second-order rate expressions as:

$$R_{i,j}^{abio} = \alpha_{i,j} C_i C_j \quad (5)$$

Where $\alpha_{i,j}$ is the second order rate coefficient for the abiotic reaction between species i and j [V/MT]. An analogous formulation is applied for the rate of oxidation of adsorbed Fe(II) and Mn(II) by dissolved oxygen, which is represented as a function of the concentration of the reduced metal adsorbed onto manganese or iron oxides and dissolved oxygen concentration:

$$R_{M^{2+},O_2}^{abio} = \alpha_{M^{2+},O_2} \{XO_2\} M^{2+} C_{O_2} \quad (6)$$

Where α_{M^{2+},O_2} is the rate coefficient for the oxidation of the adsorbed metal M^{2+} and $\{XO_2\} M^{2+}$ is the concentration of this same metal, adsorbed onto metal oxides, XO_2 [M/VT]. This adsorbed concentration is calculated either using the double layer complexation module of MINTEQA2, or by using an effective partition coefficient specified as a model input.

Precipitation and Dissolution Rate Expressions

For precipitation/dissolution reactions, a general rate expression is written following the standard collision theory relationship between the chemical reaction stoichiometry and the rate expression. For a given solid, S , composed of N_s species, the net rate of precipitation/dissolution, $R_S^{P/D}$ [M/VT], is formulated as [Smith and Jaffé, 1998]:

$$R_S^{P/D} = k_s \prod_i^{N_s} FIA_i^{\nu_{i,s}} K_{sp}^S \quad (7)$$

Where k_s is the precipitation/dissolution rate coefficient for solid S , which is a function of surface area and is experimentally specified for each mineral [reaction dependent, e.g.,

FeS: $N_s = 2$, (mol/L)⁻¹ yr⁻¹]. The ion activity product, $\prod_i^{N_s} FIA_i^{\nu_{i,s}}$, represents the

current state in the aqueous phase without considering the presence of solids, in which FIA_i is the dissolved free ion activity of component i calculated from its mass balance equation [M/V] and $\nu_{i,s}$ is the stoichiometric coefficient of the i th component of solid S .

K_{sp}^S is the equilibrium solubility product for solid S [reaction dependent, e.g., FeS: $N_s = 2$, (mol/L)²], which is inputted from the MINTEQA2 database. The corresponding net rate of change in the aqueous phase concentration for the i th dissolved component of the solid S , $R_{i,S}^{P/D}$, is calculated as $R_{i,S}^{P/D} = \nu_{i,s} R_S^{P/D}$. Equation (7) implies that precipitation proceeds when the groundwater is supersaturated with the components of the solid phase S , while dissolution of the solid phase occurs when the groundwater is undersaturated. The rate of precipitation or dissolution is proportional to the degree of over- or undersaturation.

Numerical Solution Procedure

The model consists of two parts; the dynamic transport model which considers the transport processes, the kinetically controlled biotic/abiotic reactions, precipitation and dissolution kinetics, and an equilibrium speciation model, MINTEQA2, which considers the homogeneous reactions in the aqueous phase such as speciation and complexation. Each of these two models uses the other model's solutions as input and they iterate until the solutions converge.

At the beginning of each time step, an initial solution is obtained by solving the system of coupled mass balance equations, while initially disregarding speciation and changes due to precipitation or dissolution. From this initial solution, the pE profile is estimated at each spatial node from the half reaction of the dominant terminal electron acceptor. The calculated concentration profiles, along with the pH (which is a model input) are provided to MINTEQA2 as input data to calculate the speciation of the individual species including the trace metals/radionuclides of interest at each node over the entire domain. From the information on the distribution of sorbed and dissolved species, an effective partition coefficient is determined for each dissolved species. This allows for changes in the distribution coefficient as the solution chemistry changes. Alternatively, the model also allows for the use of a constant distribution coefficient.

A second solution to the mass balance equations is then obtained by applying the effective partition coefficients obtained in the previous step and the biotic/abiotic reactions based on the previous concentration profiles. Again, using the solution from the mass balance equations as input data, the equilibrium concentration of each species is recalculated by MINTEQA2. The equilibrium solutions are compared to that of the time-dependent mass balance equations and are used to adjust total concentrations of each species. Iterations proceed until the equilibrium concentrations converge to those of the time-dependent mass balance equations.

Next, the transport system is solved again using the appropriate speciation, partitioning, biotic and abiotic reactions, and precipitation and dissolution reactions. Since the precipitation and dissolution process can affect the concentrations of related components calculated from the mass balance equations significantly, a ramping scheme is employed in the final iterative routine between the reactive transport equations and the speciation calculations in order to reduce the convergence time.

$$\frac{\partial}{\partial t} \left(K_i^{eff} \frac{\partial C_i^{eq,m}}{\partial x} \right) + \frac{\partial}{\partial x} \left(\frac{C_i^{t+1,m}}{\partial t} \frac{\partial C_{i,x}^t}{\partial x} \right) + \frac{D_{h_i}}{\partial x^2} \left(C_{i,x}^{t+1,m} - 2C_{i,x}^{t+1,m} + C_{i,x}^{t-1,m} \right) + \frac{v}{\partial x} \left(C_{i,x}^{t+1,m} - C_{i,x}^{t-1,m} \right) \quad (8)$$

$$+ \frac{1}{\partial} \left(R_i^{bio} \frac{\partial C_{i,x}^{t+1,m}}{\partial} + R_i^{abio} \frac{\partial C_{i,x}^{t+1,m}}{\partial} + R_i^{P/D} \frac{\partial C_{i,x}^{t+1,m}}{\partial} - C_i^{eq,m} \right)$$

$$\frac{C_{j,x}^{t+1,m} - C_{j,x}^t}{\partial t} + \frac{1}{\partial} \left(R_j^{bio} \frac{\partial C_{j,x}^{t+1,m}}{\partial} + R_j^{abio} \frac{\partial C_{j,x}^{t+1,m}}{\partial} + R_j^{P/D} \frac{\partial C_{j,x}^{t+1,m}}{\partial} - C_j^{eq,m} \right) \quad (9)$$

Where t , x , ∂t and ∂x are temporal and spatial indexes and increments, respectively. m is an index for the iteration at the given time step. $C_{i,x}^{t+1,m}$ is the concentration of species i at node $[x, t+1]$ at the m^{th} iteration which was updated from the previous iterative routine. $C_i^{eq,m}$ is the equilibrium concentration of species i at node $[x, t+1]$ at the m^{th} iteration estimated by MINTEQA2. ∂ is the ramping factor which is applied to

the precipitation/dissolution kinetic expression and allows the effect of precipitation /dissolution of mineral phases to be incorporated gradually into the mass balance equations. α increases from 0 to 100% by a specified fraction, based upon the convergence at each level. ϕ implies functions.

Even though this approach of coupling a transport and a chemical speciation model is computationally expensive it has the advantage of being general and allowing for the easy incorporation/substitution of additional chemical species. Furthermore, this procedure allows for an accurate fate and transport assessment in the presence of steep chemical gradients that might occur during an enhanced trace metal/radionuclide bioremediation.

Model Uncertainty Assessment

High Dimensional Model Representation (HDMR) represents a model output $f(\mathbf{x})$ as a finite hierarchical correlated function expansion in terms of the input variables x_1, x_2, \dots, x_n :

$$f(\mathbf{x}) = f_0 + \sum_{i=1}^n f_i(x_i) + \sum_{1 \leq i < j \leq n} f_{ij}(x_i, x_j) + \sum_{1 \leq i < j < k \leq n} f_{ijk}(x_i, x_j, x_k) + \dots + f_{12\dots n}(x_1, x_2, \dots, x_n) \quad (10)$$

Where f_0 is a constant representing the mean value of $f(\mathbf{x})$ in the entire domain of \mathbf{x} , and $f_i(x_i)$ gives the independent contribution to $f(\mathbf{x})$ by the input variable x_i , $f_{ij}(x_i, x_j)$ gives the pair correlated contribution of input variables x_i and x_j , and so on. The last term $f_{12\dots n}(x_1, x_2, \dots, x_n)$ contains any residual n th order correlated contribution over all input variables. The component functions of the HDMR expansion are constructed optimally, and tailored to $f(\mathbf{x})$ over the entire domain of \mathbf{x} such that the expansion converges rapidly (in many cases, to 2nd order correlated terms in Equation 10), as various trial results indicate [Shorter et al., 1999; Shorter and Rabitz, 2000; Wang et al., 1999], i.e., a satisfactory approximation of $f(\mathbf{x})$ can be given by:

$$f(\mathbf{x}) \approx f_0 + \sum_{i=1}^n f_i(x_i) + \sum_{1 \leq i < j \leq n} f_{ij}(x_i, x_j) \quad (11)$$

Various forms of HDMR have been considered with applications to a variety of scientific problems [Alis and Rabitz, 1999; Shim and Rabitz, 1998; Shorter et al., 1999; Wang et al., 1999]. Here we focus on what has been referred to as RS (Random Sampling)-HDMR. Without loss of generality, every input variable x_i can have a range [0,1] after some proper transformation. Let C^k represent the k -dimensional unit hypercube. The formulas of RS-HDMR component functions in Equation 10 are as follows:

$$\begin{aligned} f_0 &= \int_{C^n} f(\mathbf{x}) d\mathbf{x} \\ f_i(x_i) &= \int_{C^{n-1}} f(\mathbf{x}) d\mathbf{x}^i - f_0 \quad i = 1, 2, \dots, n \\ f_{ij}(x_i, x_j) &= \int_{C^{n-2}} f(\mathbf{x}) d\mathbf{x}^{ij} - f_i(x_i) - f_j(x_j) + f_0, \quad 1 \leq i < j \leq n \end{aligned} \quad (12)$$

where $d\mathbf{x} = dx_1 dx_2 \dots dx_n$, and $d\mathbf{x}^i$, $d\mathbf{x}^{ij}$ are just $d\mathbf{x}$ without elements dx_i and $dx_i dx_j$, respectively. Considering that C^n is a hypercube, f_0 is the mean value of \bar{f} of $f(\mathbf{x})$.

The component functions of RS-HDMR are mutually orthogonal to permit the model output variance $\sigma_{\bar{f}}^2$ to be decomposed into its input variable statistical contributions due to the independent action of the variables σ_i^2 , the pair correlated action σ_{ij}^2 , etc.

$$\begin{aligned} \sigma_{\bar{f}}^2 &= \int_{C^n} [f(\mathbf{x}) - \bar{f}]^2 d\mathbf{x} = \int_{C^n} [f(\mathbf{x}) - f_0]^2 d\mathbf{x} \\ &= \int_{i=1}^n \int_0^1 f_i^2(x_i) dx_i + \int_{i \neq j}^n \int_0^1 \int_0^1 f_{ij}^2(x_i, x_j) dx_i dx_j + \dots \\ &= \int_{i=1}^n \sigma_i^2 + \int_{i \neq j}^n \sigma_{ij}^2 + \dots \end{aligned} \quad (13)$$

The determination of σ_i^2 , σ_{ij}^2 , ... requires the evaluation of the integrals $\int f_i^2(x_i) dx_i$, $\int f_{ij}^2(x_i, x_j) dx_i dx_j$, etc. Monte Carlo integration is used for these evaluations [Press et al., 1992]. For instance, a set of N n -dimensional vectors $\{x_1^s, x_2^s, \dots, x_n^s\}$, $s = 1, 2, \dots, N$ is randomly generated to yield:

$$f_0 = \int_{C^n} f(\mathbf{x}) d\mathbf{x} = \frac{1}{N} \sum_{s=1}^N f(\mathbf{x}^s) \quad (14)$$

$$\sigma_{\bar{f}}^2 = \int_{C^n} [f(\mathbf{x}) - f_0]^2 d\mathbf{x} = \frac{1}{N} \sum_{s=1}^N [f(\mathbf{x}^s) - f_0]^2 \quad (15)$$

When $N \rightarrow \infty$, the limit values of f_0 , $\sigma_{\bar{f}}^2$ can be obtained. Very often the Monte Carlo integration converges sufficiently fast for modest values of N .

The functions $f_i(x_i)$, $f_{ij}(x_i, x_j)$, ... can be approximately represented as linear combinations of orthonormal polynomials $\phi_k(x_i)$, which gives:

$$f(\mathbf{x}) = f_0 + \sum_{i=1}^n \sum_{k=1}^r c_k^i \phi_k(x_i) + \sum_{i \neq j}^n \sum_{k=1}^r \sum_{l=1}^r c_{kl}^{ij} \phi_k(x_i) \phi_l(x_j) + \dots, \quad (16)$$

where

$$\begin{aligned} \phi_1(x) &= a_1 x + a_2, \\ \phi_2(x) &= b_1 x^2 + b_2 x + b_3, \\ \phi_3(x) &= c_1 x^3 + c_2 x^2 + c_3 x + c_4, \\ &\dots \end{aligned}$$

are mutually orthogonal with zero mean and unit norm. Their coefficients are determined by an optimization procedure for different random sample sizes to assure their orthogonality. The resultant $\phi_k(x_i)$ are called optimal orthonormal polynomials. In most cases, acceptable accuracy may be achieved using $\phi_1(x)$, $\phi_2(x)$ and $\phi_3(x)$ (i.e., $r = 3$).

Since $\phi_k(x_i)$ are mutually orthogonal for all i , k and l , the coefficients c_k^i and c_{kl}^{ij} can be determined by Monte Carlo sampling as:

$$c_k^i = \frac{1}{N} \sum_{s=1}^N f(\mathbf{x}^s) \varphi_k(x_i^s) \quad (17)$$

$$c_{kl}^{ij} = \frac{1}{N} \sum_{s=1}^N f(\mathbf{x}^s) \varphi_k(x_i^s) \varphi_l(x_j^s) \quad (18)$$

Then, σ_i^2 and σ_{ij}^2 are simply the sums of $(c_k^i)^2$ for all k , and the sums of $(c_{kl}^{ij})^2$ for all k and l , respectively.

$$\sigma_i^2 = \sum_{k=1}^r (c_k^i)^2 \quad (19)$$

$$\sigma_{ij}^2 = \sum_{k=1}^r \sum_{l=1}^r (c_{kl}^{ij})^2 \quad (20)$$

Notice that only one randomly sampled set of $f(\mathbf{x}^s)$ is needed to determine f_0 , $f_i(x_i)$, $f_{ij}(x_i, x_j)$, ... and consequently, σ_f^2 , σ_i^2 , σ_{ij}^2 , etc, and the assessments are valid for the whole domain of \mathbf{x} . This makes global uncertainty assessments of a model very efficient. Moreover, RS-HDMR provides not only quantitative assessments σ_f^2 , σ_i^2 , σ_{ij}^2 , ..., but also the qualitative behaviors of the independent and collective actions $f_i(x_i)$, $f_{ij}(x_i, x_j)$, ... of the input variables on the output. Hence, the uncertainty assessment given by RS-HDMR is valuable for attaining a physical understanding of the origins of output uncertainty as well as suggestions for modification of the model and additional laboratory or field studies to best improve the quality of the model [Li *et al.*, manuscript in preparation].

Model Application and Discussion

Model Application to the Fate and Transport of Uranium in the Subsurface

Under oxidizing conditions the dominant form of uranium is U(VI) as in the oxide UO_3 and/or the yellow uranyl ion UO_2^{2+} which are highly soluble and mobile, while under reducing conditions uranium forms insoluble phases such as uraninite and/or coffinite in the form of U(IV). Although uranium may also exist as U(III) and also U(V), the respective ions are unstable and not common in groundwater environments. Complexation of U(VI) with carbonates may affect its sorption onto the solid matrix significantly, especially at high pH values or at high CO_2 partial pressures [Zeh *et al.*, 1997]. This effect is accounted for in the model formulation when the lumped partition coefficients are estimated based on the computed speciation of the different species in solution.

The reduction of U(VI) can be caused by biotic and abiotic reactions. Some Fe(III)- and sulfate-reducing bacteria are capable of reducing uranium under anaerobic conditions by using U(VI) as a terminal electron acceptor during the oxidation of an organic substrate [Lovley, 1997; Truex *et al.*, 1997; Tucker *et al.*, 1998]. The thermodynamic energy yield from the reduction of U(VI) to U(IV) is -63.3 kcal/mol and to U(III) is -52.2 kcal/mol, which is twice that of Fe(III) reduction. Based on the thermodynamic energy yield, uranium reduction should occur in the sequence of $\text{Mn(IV)} > \text{U(VI)} > \text{Fe(III)}$ [Francis *et al.*, 1994]. Since U(VI) is an electron acceptor with a relatively low concentration it may

be utilized simultaneously with electron acceptors that are more readily available. Therefore, in the model formulations presented here, we assumed that after Mn(IV) is used up through biotic/abiotic redox reactions, biologic uranium reduction occurs simultaneously with Fe(III) reduction, and after the bioavailable Fe(III) has been consumed it may continue simultaneously with sulfate reduction. U(VI) can also be reduced via abiotic reactions such as by Fe(II) sorbed onto iron corrosion products like hematite [Charlet *et al.*, 1998]. On the other hand, U(IV) can be oxidized to U(VI) in oxic solutions or in the presence of nitrate. The consumption/production of U(VI) and U(IV) is described as:

$$R_{U6} = \mu_{O,U4} \left(1 - \frac{C_{O,U4}}{C_O} \right) \frac{C_{U6}}{K_{s,U6} + C_{U6}} \frac{C_C}{K_{s,C} + C_C} \quad (21)$$

$$R_{U4} = \frac{\mu_{U6,Fe2[ad]} K_{d,Fe2}^{eff} C_{Fe2} C_{U6}}{1 + \mu_{U6,Fe2[ad]} K_{d,Fe2}^{eff} C_{Fe2} C_{U6}} \frac{C_{U6}}{K_{s,U6} + C_{U6}} \frac{C_C}{K_{s,C} + C_C} - \mu_{U6,Fe2[ad]} K_{d,Fe2}^{eff} C_{Fe2} C_{U6} \quad (22)$$

Where $\mu_{m,C,U6}$ is the maximum biologic rate of organic substrate oxidation when U(VI) is the electron acceptor [M/TV]. K_C and K_{U6} are the half-saturation coefficients for the biologic degradation of the organic substrate and U(VI), respectively. $\mu_{O,U4}$ and $\mu_{U6,Fe2[ad]}$ are the second order rate coefficient for the abiotic reactions of oxygen/U(IV) and U(VI)/sorbed Fe(II), respectively [V/MT]. C_O , C_C , C_{Fe2} , C_{U6} and C_{U4} are the dissolved concentrations of oxygen, organic substrate, Fe(II) and U(VI) and the solid concentration of U(IV), respectively. μ_{Fe3} is the indicator coefficient for Fe(III) utilization and $\mu_{U6,C}$ is the stoichiometric coefficient representing the ratio of the number of moles of U(VI) required to oxidize one mole of organic substrate. $K_{d,Fe2}$ is the partition coefficient of Fe(II). Although much research has been conducted on the biological reduction of uranium in recent years, no direct measurements of the reaction rate coefficients required for the formulation described above have been reported in the literature. For the simulations conducted here, rate coefficients of uranium were therefore inferred from experimental observations described by several investigators [Francis *et al.*, 1994; Lovley, 1997; Truex *et al.*, 1997; Tucker *et al.*, 1998; Charlet *et al.*, 1998], and are given in Table 1.

A series of numerical experiments were conducted to assess the dynamics of uranium in a saturated aquifer during bioremediation. Model input parameters used in these simulations are given in Table 2. Prior to biostimulation, it was assumed that the aquifer is contaminated by U(VI) with a concentration of 0.1 mol/L. A series of electron acceptors with specified concentration were assumed to exist in the system at $t = 0$. Simulations were conducted for acetate injection into the groundwater resulting in an organic carbon concentration of $3 \cdot 10^3$ mol/L, for $t > 0$ upstream of the domain's boundary. Upstream constant flux boundary conditions were used for all species in the numerical simulations. At the outflow of the domain, zero gradient boundary conditions were used.

Table 1. Key biotic/abiotic reaction parameters used in the simulation

	value	values in literature
Maximum rate of organic substrate oxidation when [mol/L/yr]		
O ₂ is the electron acceptor	0.1	4.3 ? 10 ⁻⁴ (7) – 1 (5)
NO ₃ ⁻ is the electron acceptor	0.004	4.6 ? 10 ⁻⁴ (7) – 0.04 (5)
Mn(IV) is the electron acceptor	0.001	3.3 ? 10 ⁻⁴ (7) – 0.01 (5)
Fe(III) is the electron acceptor	0.0005	1.2 ? 10 ⁻³ (7) – 0.005 (5)
U(VI) is the electron acceptor	0.0002	–
SO ₄ ²⁻ is the electron acceptor	0.017	0.17 (5)
CO ₂ is the electron acceptor: methanogenesis	0.05	0.05 (5)
Half saturation constant of [?mol/L]		
organic carbon	54	100 (5,6)
O ₂	20	15.8 (7) – 20 (5,6)
NO ₃ ⁻	20	15.8 (7) – 20 (5,6)
Mn (IV)	3.7	0.4 (7) – 2 (5,6)
Fe (III)	3.7	2 (5,6) – 63.1 (7)
U(VI)	0.1	–
SO ₄ ²⁻	10	10 (5,6)
Threshold concentrations [?mol/L] for indicator ? _{ea}		
O ₂	0.5	0.5 (5) – 30 (2)
NO ₃ ⁻	6	0.6 (5) – 80 (2)
Mn (IV)	1	0.9 (5) – 74 (1)
Fe (III)	5	90 (5)
SO ₄ ²⁻	15	15 (5)
Maximum utilization rate of [yr ⁻¹]		
ammonia oxidation (nitrification)	30	30 (5,6)
aerobic methane oxidation	10	10 (5,6)
Half saturation constant of [?mol/L]		
ammonia oxidation (nitrification)	30	30 (5,6)
aerobic methane oxidation	10	10 (5,6)
Second-order rate coefficients for the redox reactions [(mol/L)/yr]		
Oxidants	Reductants	
MnO ₂ (s)	Fe(II)	1.0 ? 10 ⁸ 1.0 ? 10 ⁴ (5,6) – 1.0 ? 10 ⁹ (2,3)
MnO ₂ (s)	HS ⁻	1.0 ? 10 ⁸ 8.0 ? 10 ⁵ (5,6) – 1.0 ? 10 ⁸ (2,3)
FeOOH (s)	HS ⁻	1.0 ? 10 ³ 1.0 ? 10 ³ (5,6) – 8.0 ? 10 ³ (4)
O ₂ (aq)	XMn ²⁺ (ads)	2.1 ? 10 ⁷ 2.1 ? 10 ⁷ (5,6)
O ₂ (aq)	XFe ²⁺ (ads)	1.0 ? 10 ³ 6.0 ? 10 ⁴ (4) – 1.6 ? 10 ⁸ (5,6)
O ₂ (aq)	Fe(II)	2.1 ? 10 ⁷ 2.1 ? 10 ⁷ (4) – 2.0 ? 10 ⁹ (2,3)
O ₂ (aq)	Mn(II)	4.6 4.6 (5) – 1.0 ? 10 ⁷ (4)
O ₂ (aq)	U(IV)	1.0 ? 10 ¹ –
O ₂ (aq)	HS ⁻	2.0 ? 10 ⁵ 2.0 ? 10 ⁵ (5,6)
NO ₃ ⁻	Fe(II)	1.6 ? 10 ³ 1.6 ? 10 ³ (6)
U(VI)	XFe ²⁺ (ads)	5.0 ? 10 ⁴ –
[SO ₄ ⁻] _{total}	CH ₄	1.0 ? 10 ² 1.0 ? 10 ⁴ (5,6)

(1) Essaid et al., 1995; (2) Van Cappellen and Wang, 1995; (3) Van Cappellen and Wang, 1996; (4) Hunter et al. 1998; (5) Smith and Jaffé, 1998; (6) Kallin, 1999; (7) Abrams and Loague, 2000

Table 2. Model input parameters used in the simulation

	value	unit
domain length	30	[m]
groundwater velocity	10	[m yr ⁻¹]
dispersivity	25	[cm]
porosity	0.35	
dry bulk density of soil	2.0	[g cm ⁻³]
pH	6.5	
	[?mol/L]	initial conditions
		Dissolved concentrations upstream of the domain's boundary
Organic carbon	0	3,000 t > 0
O ₂	100	100
NO ₃ ⁻	200	200
Mn (IV)	25	0
Fe (III)	50	0
U(VI)	0.1	0.1
SO ₄ ²⁻	300	300

The effect of the aquifer biostimulation via the injection of the carbon source on U(VI) reduction can be seen in Figure 1 for time increments of 0.2 years, up to a one-year period. After the carbon source is injected at the origin, the U(VI) concentration steadily decreases. The concentration of U(IV) increases significantly at about 1m from the origin as time progresses. The reason is that at this distance, and for the conditions simulated, oxygen and nitrate, which both are entering the domain at the upstream boundary, as well as the initial amount of Mn(IV) have all been utilized in the degradation of the organic substrate, allowing the utilization of U(VI) to start at this point, which then precipitates as U(IV). Furthermore, since no oxidants reach the zone where the U(VI) precipitated, the precipitate remains stable and is not reoxidized into U(VI). No biological uranium reduction takes place until all the Mn(IV) has been consumed. Some U(IV) can precipitate where more favorable electron acceptors still exist due to the abiotic reduction of U(VI) by sorbed Fe(II). It is important to note that most of the mass of the organic substrate injected reacts with the incoming electron acceptors. Hence, a bioremediation scheme as described here is a reactive barrier for the incoming uranium.

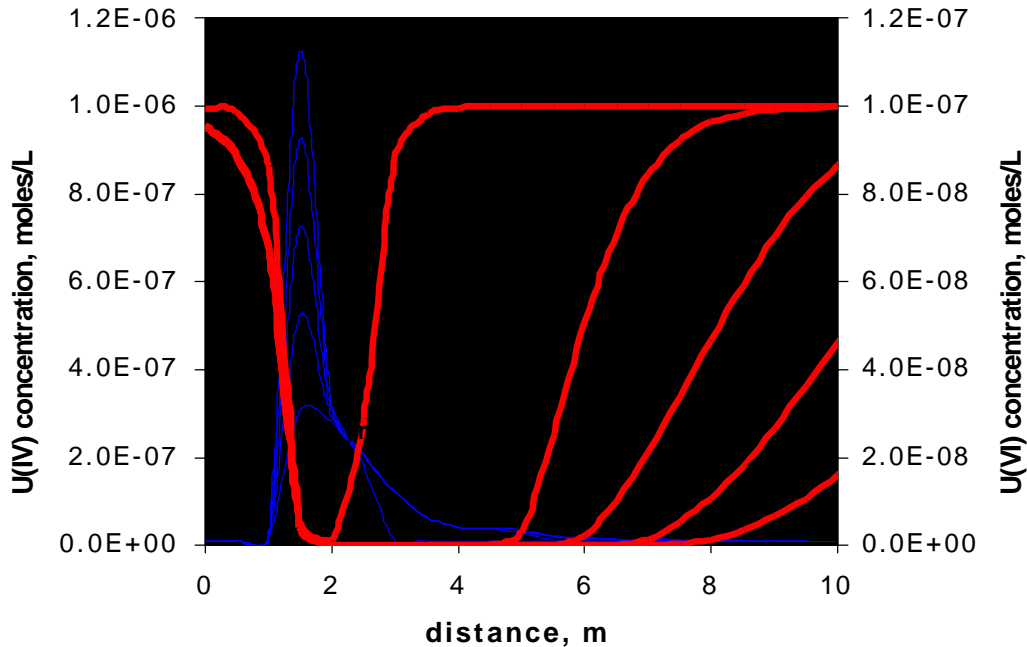


Figure 1. Simulated concentration profiles of U(IV) and U(VI) over 1 year of biostimulation

As discussed earlier, U(VI) can act as an electron acceptor for certain bacteria during the degradation of organic matter. As opposed to the major electron acceptors described in the model, U(VI) reduction was allowed to proceed in parallel with the reduction of the other electron acceptors after Mn(IV) has been consumed. For this reason U(VI) reduction proceeds even when the environment becomes highly reduced

and methanogenesis occurs. Further research is necessary to establish if there is a lower redox limit for the reduction of U(VI).

Model Uncertainty Assessments by RS-HDMR

A model analysis was performed to determine the relative importance of the different reactions onto the performance of a uranium bioremediation scheme. The global output uncertainty for uranium bioremediation simulations over the entire simulation domain of 13 input variables was quantified by RS-HDMR using only 300 model runs with randomly sampled input variables. The global uncertainty assessments with respect to 13 input variables are presented for two model outputs: (1) cumulative flux of U(VI) passing through a given distance from the origin after the organic substrate was introduced (F_U), and (2) concentration of U(VI) at a given distance from the origin (C_U). The 13 biotic and abiotic reaction rate coefficients as well as their dynamic range used in the analysis are given in Table 3.

A set of 300 model input vectors of $\mathbf{x}^s = [x_1^s, x_2^s, \dots, x_{13}^s]$ ($s = 1, 2, \dots, 300$) within the ranges shown in Table 3 was generated utilizing a quasi-random sampling method [Press, 1992]. The remaining model parameters were maintained constant at the values shown in Tables 1 and 2. The corresponding outputs F_U and C_U for \mathbf{x}^s at different distances from the origin ($d = 1, 2, \dots, 30m$) were obtained by conducting the corresponding model simulations. Using these data, the mean values \bar{F}_U, \bar{C}_U and the total variances $\sigma_{\bar{F}_U}^2, \sigma_{\bar{C}_U}^2$ were calculated. Due to the relatively small sample size of 300 points, only the first order standard deviations σ_i for F_U and C_U were calculated at different distances from the origin by the RS-HDMR method, and the 1st order RS-HDMR component functions $f_i(x_i)$ were approximated by the 3rd order optimal orthonormal polynomial expansion.

The uncertainty assessments for the cumulative flux of U(VI), F_U , were performed at different distances ($d = 1, 2, \dots, 30m$) and, as an example, the results at $d = 2m$ are given in Table 4. The mean value of F_U for the 300 samples is $f_0 = 0.168 \cdot 10^{24}$ (mol/L · cm²). The results given in Table 4 show that $\sigma_{\bar{F}_U}$ and $\sqrt{\sigma_i^2}$ for different sample sizes do not differ very much and the convergence is good even if the sample sizes are as small as 100. Moreover, $\sigma_{\bar{F}_U}$ and $\sqrt{\sigma_i^2}$ of the sample are quite close to each other (e.g., for 300 samples, the value of $\sqrt{\sigma_i^2}$ is 80% of the value of $\sigma_{\bar{F}_U}$), which implies that the higher order correlation actions between variables are small. The largest σ_i, σ_2 , is the same for the three different sample sizes examined. The σ_i for the remaining input variables are relatively small and their orders and contributions to the output do not appear very important. Hence the results obtained from the 300 points provide a reliable analysis of the model. The values of $f_0, \sigma_{\bar{F}_U}$ and $\sqrt{\sigma_i^2}$ determined using the sample size of 300 are given in Figure 2 as a function of the distance from the origin.

Table 3. The biotic/abiotic input variables and their ranges in the analysis

input variables			random sampling range		
No.	Description		minimum	maximum	
maximum rate of organic carbon oxidation [mol/L/yr] when					
1	O ₂ is the electron acceptor	? _{m,C,O}	0.01	1.0	
2	NO ₃ ⁻ is the electron acceptor	? _{m,C,N}	0.0004	0.04	
3	Mn(IV) is the electron acceptor	? _{m,C,M}	0.0001	0.01	
4	Fe(III) is the electron acceptor	? _{m,C,F}	0.00005	0.005	
5	U(VI) is the electron acceptor	? _{m,C,U}	0.00002	0.002	
6	SO ₄ ²⁻ is the electron acceptor	? _{m,C,S}	0.0017	0.17	
7	CO ₂ is the electron acceptor: methanogenesis	? _{m,C,Me}	0.0005	0.05	
Second-order rate coefficients for the redox reactions [(mol/L) ⁻¹ /yr]					
	oxidants	reductants			
8	O ₂	U(IV)	? _{OU 4}	1 ? 10 ⁰	1 ? 10 ²
9	[SO ₄ ²⁻] _{total}	CH ₄	? _{SO4,CH 4}	1 ? 10 ¹	1 ? 10 ³
10	U(VI)	XFe ²⁺ (ads)	? _{U 6,Fe 2[ad]}	5 ? 10 ³	5 ? 10 ⁵
11	O ₂	XFe ²⁺ (ads)	? _{O,Fe 2[ads]}	1 ? 10 ²	1 ? 10 ⁴
12	MnO ₂ (s)	HS ⁻	? _{Mn 4,HS}	1 ? 10 ⁷	1 ? 10 ⁹
13	MnO ₂ (s)	Fe(II)	? _{Mn 4,Fe 2}	1 ? 10 ⁷	1 ? 10 ⁹

Table 4. The order of standard deviations σ_i , $\sigma_{\bar{F}_U}$ and $\sqrt{\sigma_i^2}$ for output F_U at $d = 2m$ obtained from different input variables and different data sizes

Sample size					
100		200		300	
x_i	σ_i	x_i	σ_i	x_i	σ_i
2	0.119×10^{-4}	2	0.119×10^{-4}	2	0.128×10^{-4}
7	0.363×10^{-5}	4	0.204×10^{-5}	4	0.211×10^{-5}
6	0.353×10^{-5}	12	0.191×10^{-5}	5	0.156×10^{-5}
8	0.348×10^{-5}	6	0.187×10^{-5}	7	0.150×10^{-5}
12	0.332×10^{-5}	13	0.176×10^{-5}	6	0.143×10^{-5}
9	0.248×10^{-5}	5	0.175×10^{-5}	13	0.124×10^{-5}
4	0.244×10^{-5}	7	0.146×10^{-5}	11	0.111×10^{-5}
1	0.241×10^{-5}	9	0.144×10^{-5}	12	0.102×10^{-5}
13	0.212×10^{-5}	8	0.107×10^{-5}	10	0.961×10^{-6}
10	0.158×10^{-5}	10	0.909×10^{-6}	8	0.837×10^{-6}
3	0.967×10^{-6}	3	0.765×10^{-6}	1	0.610×10^{-6}
5	0.835×10^{-6}	1	0.761×10^{-6}	9	0.516×10^{-6}
11	0.815×10^{-6}	11	0.551×10^{-6}	3	0.474×10^{-6}
$\sigma_{\bar{F}_U}$	0.163×10^{-4}	$\sigma_{\bar{F}_U}$	0.162×10^{-4}	$\sigma_{\bar{F}_U}$	0.169×10^{-4}
$\sqrt{\sigma_i^2}$	0.148×10^{-4}	$\sqrt{\sigma_i^2}$	0.129×10^{-4}	$\sqrt{\sigma_i^2}$	0.135×10^{-4}

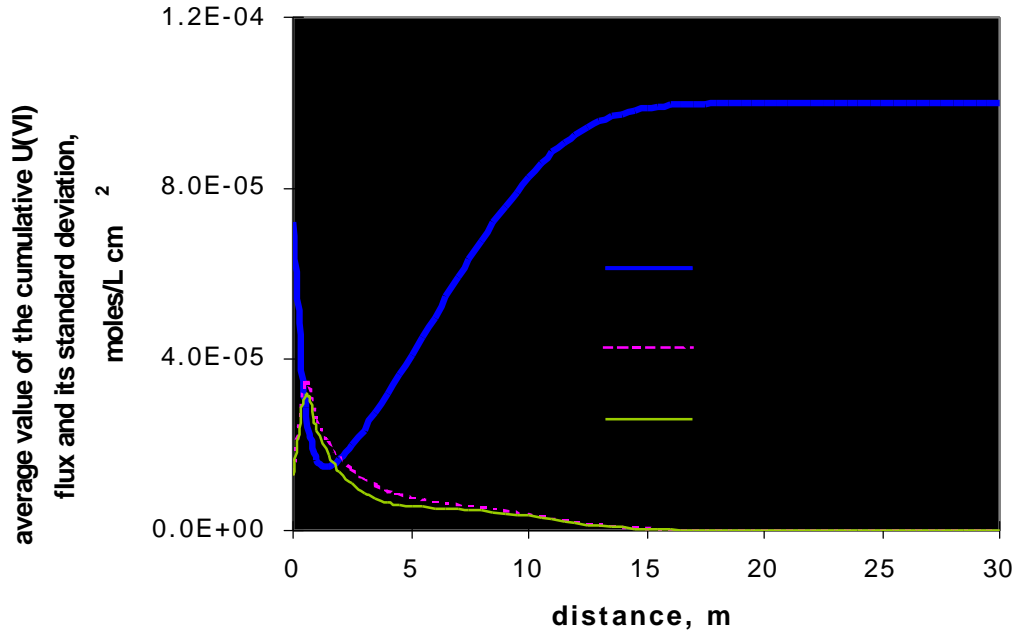


Figure 2. Estimated values of, \bar{F}_U , and $\sqrt{\sum \sigma_i^2}$ of the cumulative U(VI) flux (F_U) over 1 year of biostimulation as a function of the distance from the origin

The contributions to the standard deviation $\sigma_{\bar{F}_U}$ of each of the 13 inputs analyzed, σ_i , as a function of the distance from the origin, are shown in Figure 3. The output uncertainty is largest in the locations where active uranium reduction occurs, while at distances far from the origin the output uncertainty is zero, as one would expect. The results shown in Figure 3 and Table 4 reveal that for output F_U , input 2 (the biotic nitrate-reducing rate coefficient) is the rate coefficient that has the largest impact on the flux of uranium over most of the relevant spatial domain. This result is reasonable considering that, according to the model formulation, uranium cannot be reduced until all oxygen, nitrate, and manganese have been consumed. Given the relative concentrations of these electron acceptors and their utilization rates, nitrate will take longest to be completely utilized. As the distance from the origin increases, the reaction time for nitrate reduction has increased, and nitrate depletion is less sensitive to the nitrate reduction rate, which is shown by its decreasing contribution to the overall output uncertainty. In this region the uranium reduction rate has about as big an influence on the model output as the nitrate reduction rate. Finally it is interesting to note that, at the leading edge of the domain where bioremediation occurs, $d > 8\text{m}$, the U(VI) flux is about equally sensitive to the nitrate, iron, uranium and sulfate reduction rates. The reason for this is that uranium reduction mainly occurs between $1\text{m} < d < 3\text{m}$ and the U(VI) flux

downstream of this zone is significantly affected by the processes occurring upstream of that location.

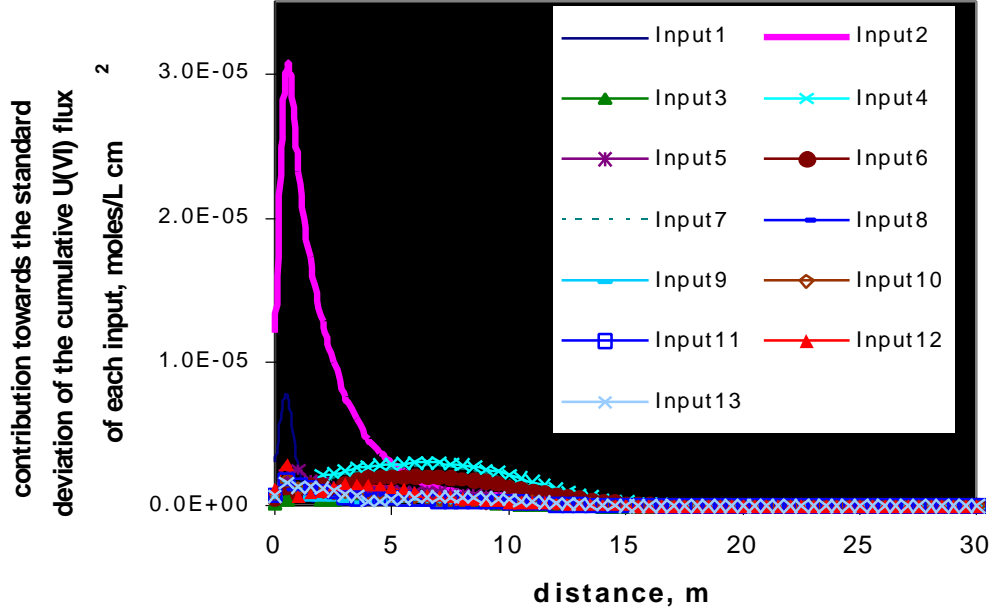


Figure 3. Contributions, σ_i , to the standard deviation $\sigma_{\bar{C}_U}$ of each of the 13 inputs analyzed

The uncertainty assessment for the concentration of U(VI), C_U , was performed at different distances from the origin, and the results at $d \geq 2m$ are given in Table 5. The mean value of C_U for the 300 samples is $f_0 \approx 0.420 \cdot 10^{18} \text{ mol/L}$. The results presented in Table 5 show that, similarly to the results for F_U , the estimated values of $\sqrt{\sigma_i^2}$ for the three different sample sizes do not differ very much and are close to $\sigma_{\bar{C}_U}$ (e.g., for 300 samples, the value of $\sqrt{\sigma_i^2}$ is 74% of the value of $\sigma_{\bar{C}_U}$). This implies that the first order terms are dominant, and again indicates that there are only small higher order correlation actions among the variables that affect C_U . The largest σ_i , σ_2 , is the same for the three different sample sizes examined. The σ_i for the remaining input variables are relatively small and their orders and contributions to the output do not appear very important. The values of f_0 , $\sigma_{\bar{C}_U}$ and $\sqrt{\sigma_i^2}$ as a function of the distance from the origin for the output C_U are shown in Figure 4, and the respective values of σ_i for the thirteen rate coefficients investigated are shown in Figure 5. The results show that for $0m < d < 5m$ nitrate reduction has by far the highest contribution, σ_i , to the total $\sigma_{\bar{C}_U}$. In the

region $5\text{m} < d < 15\text{m}$ the methanogenesis rate has the highest contribution, σ_i , to $\sigma_{\bar{C}_U}$ followed by the iron reduction rate and sulfate reduction rate.

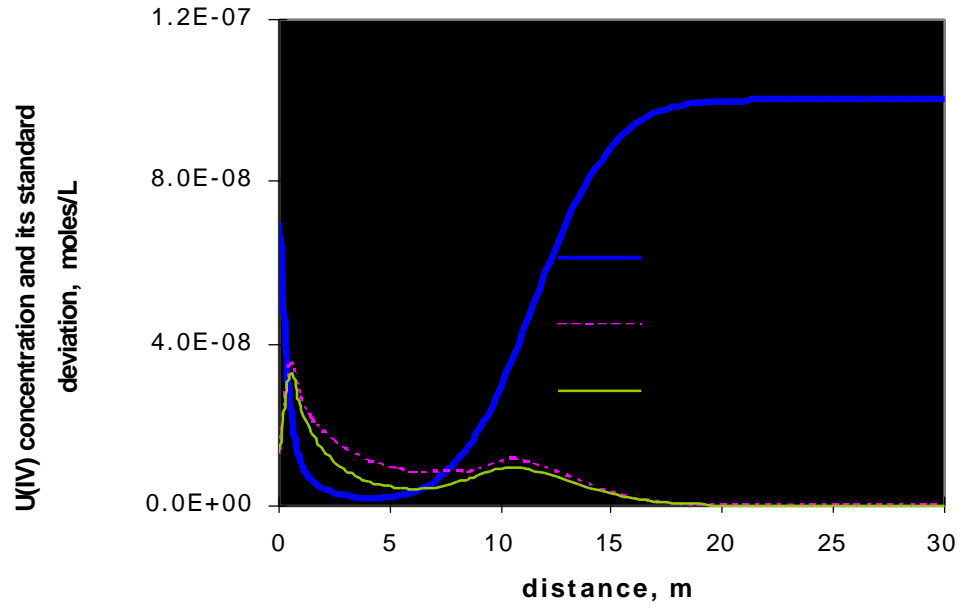


Figure 4. Estimated values of, σ and $\sqrt{\sigma \sigma_i^2}$ of the U(VI) concentration (C_U) at $t = 1$ year as a function of the distance from the origin

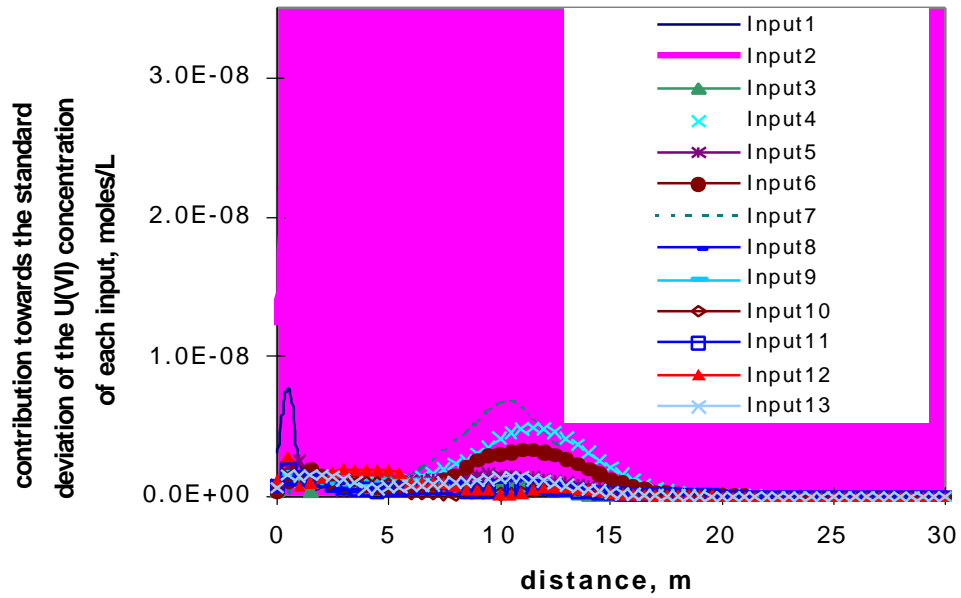


Figure 5. Contributions, σ_i , to the standard deviation $\sigma_{\bar{C}_U}$ of each of the 13 inputs analyzed

Table 5. The order of standard deviations σ_i , $\sigma_{\bar{C}_U}$ and $\sqrt{\sigma_i^2}$ for output C_U at $d \approx 2m$ obtained from different input variables and different data sizes

Sample size					
100		200		300	
x_i	σ_i	x_i	σ_i	x_i	σ_i
2	0.118×10^{-7}	2	0.118×10^{-7}	2	0.129×10^{-7}
8	0.394×10^{-8}	12	0.223×10^{-8}	13	0.157×10^{-8}
12	0.364×10^{-8}	13	0.200×10^{-8}	6	0.157×10^{-8}
7	0.362×10^{-8}	9	0.180×10^{-8}	4	0.153×10^{-8}
6	0.323×10^{-8}	8	0.145×10^{-8}	7	0.150×10^{-8}
9	0.278×10^{-8}	5	0.143×10^{-8}	5	0.136×10^{-8}
1	0.270×10^{-8}	4	0.140×10^{-8}	12	0.133×10^{-8}
13	0.239×10^{-8}	6	0.134×10^{-8}	3	0.119×10^{-8}
4	0.229×10^{-8}	10	0.126×10^{-8}	11	0.118×10^{-8}
10	0.223×10^{-8}	7	0.122×10^{-8}	10	0.108×10^{-8}
5	0.133×10^{-8}	1	0.105×10^{-8}	9	0.992×10^{-9}
8	0.130×10^{-8}	3	0.102×10^{-8}	8	0.967×10^{-9}
11	0.994×10^{-9}	11	0.790×10^{-9}	1	0.733×10^{-9}
$\sigma_{\bar{C}_U}$	0.176×10^{-7}	$\sigma_{\bar{C}_U}$	0.176×10^{-7}	$\sigma_{\bar{C}_U}$	0.184×10^{-7}
$\sqrt{\sigma_i^2}$	0.151×10^{-7}	$\sqrt{\sigma_i^2}$	0.128×10^{-7}	$\sqrt{\sigma_i^2}$	0.136×10^{-7}

It is interesting to evaluate the results shown in Figures 3 and 5 in more detail. These figures show for the two model outputs, U(VI) flux and U(VI) concentration, the mean value and the standard deviation of simulated outputs. The coefficient of variation, which is the standard deviation over the mean value, can be viewed as a simple measure to determine the uncertainty of the model output, with higher coefficients of variation implying a higher uncertainty. It is easy to see that for the computed flux, the coefficient of variation remains below 1 for the entire spatial domain, while for the computed concentration the coefficient of variation is larger than 1 for $1.5 \text{ m} < d < 10 \text{ m}$, reaching values on the order of 16. For the computed uranium concentrations, these high coefficients of variation are exactly in the location where the uranium reduction is expected to take place, indicating that small changes in the dominant rate coefficients will significantly affect the uranium concentration at a given location and time. In contrast, the estimated fluxes, which are an integration of the point flux over time, have a smaller uncertainty associated with them.

Finally it should be pointed out that since the model incorporates biomass into the kinetic coefficients the effects of biological lag time and buildup of biomass are not shown in these analyses. A separate simulation, in which the specific growth rates were increased linearly from 0 to their maximum value over a 40-day period, showed a slightly more skewed U(IV) profile, but did not have a major effect on the results of the one-year simulations.

Conclusions

This study presents a numerical model for simulating the biogeochemical dynamics of trace metals, metalloids, and radionuclides, in saturated porous media under biostimulation via the injection of a carbon source. A system of mass balance equations for the electron donor(s) and acceptors, reduced species, and trace metal/radionuclide of interest, coupled via the appropriate biotic and/or abiotic reaction terms was constructed and solved numerically using a finite difference approximation. Redox profiles, which develop in response to the sequential utilization of various terminal electron acceptors during the biodegradation of the organic substrate were simulated and coupled with the dynamics of uranium in order to illustrate the enhanced biological reduction of U(IV) and in situ immobilization as the solid-phase U(VI).

The reaction kinetics can have significant impacts on the individual chemical profiles. When the water flow is from the oxidized zone to the reduced zone, the electron acceptors are depleted sequentially. Conversely, when the water flows from reduced to more oxidized zones, the various biotic and abiotic reactions occurring simultaneously can alter the spatial sequence of the profiles of the electron acceptors. This, as well as the overlapping concentration profiles, illustrates that knowledge of the electron acceptor profiles alone does not provide adequate information to identify the zones where a specific microbiological process is occurring.

A new tool for model analysis, global uncertainty assessments based on RS-HDMR, is presented and applied to identify the key processes affecting the bioremediation of uranium-contaminated aquifers, based on the model presented here. With a modest size of random samples, RS-HDMR can efficiently provide a reliable global uncertainty assessments for a model. Its advantages come from the properties of RS-HDMR in that the high-dimensional input-output systems can be approximated very well with a relatively small input-output sample, and that the individual RS-HDMR component functions have a direct statistical correlation interpretation. The first property dramatically reduces the sampling effort. The second one permits the model output variance σ^2 to be decomposed into its input contributions σ_i^2 , σ_{ij}^2 , etc. due to

the independent variable action σ_i^2 , the pair correlation action σ_{ij}^2 , etc. The information gained from this decomposition can be most valuable for attaining a physical understanding of the origins of output uncertainty as well as suggestions for additional laboratory/field studies or parameter/process formulation refinements to best improve the quality of the model. As shown in the analysis, a fully global uncertainty assessment of the model required only a modest set of output data for randomly sampled inputs of all the kinetic coefficients evaluated. Hence, RS-HDMR is a practical approach for model uncertainty assessment.

Given the lack of data for model validation, the model presented here needs further testing and possible upgrading prior to using it for design purposes. The model and model analysis performed are nevertheless valuable as a scientific tool to understand variable interactions, and to be used as an aid in designing field tests as well as interpreting field observations. The results of the model analysis clearly demonstrate that it is extremely important to properly predict the dynamics of nitrate reduction in order to accurately estimate where and when uranium will be reduced. Since uranium ore is commonly extracted with nitric acid, high levels of nitrate are typical in uranium-contaminated groundwater, and this conclusion applies therefore to most sites where bioremediation of such aquifers is considered.

III. PRELIMINARY SIMULATIONS IN SUPPORT OF URANIUM BIOREMEDIATION AT UMTRA SITES

Table 6. Key rate parameters used in the UMTRA simulations

$\lambda_{O,U(IV)}$	=	1.0×10^4 / yr
$\lambda_{Fe(II)}$	=	0.31
$\lambda_{m,C,U(VI)}$	=	0.02 mole / L·yr
$K_{s,U(VI)}$	=	1.32×10^{-4} mole / L
$K_{s,C}$	=	1.00×10^{-6} mole / L
$\lambda_{U(VI),Fe(II)[ad]}$	=	1.0×10^5 / yr
λ_{acc}	: acclimation factor. (0 \rightarrow 1 for 30 days linearly)	

Table 7. Initial aquifer conditions and concentrations at the origin during biostimulation

	Initial condition mol/L	Inflowing concentration mol/L
Acetate	0	6
Oxygen	3.13	3.13
Nitrate	10	10
Mn(III)	5	0
Fe(III)	50	0
Sulfate	100	100
U(VI)	3	3
U(IV)	0	0

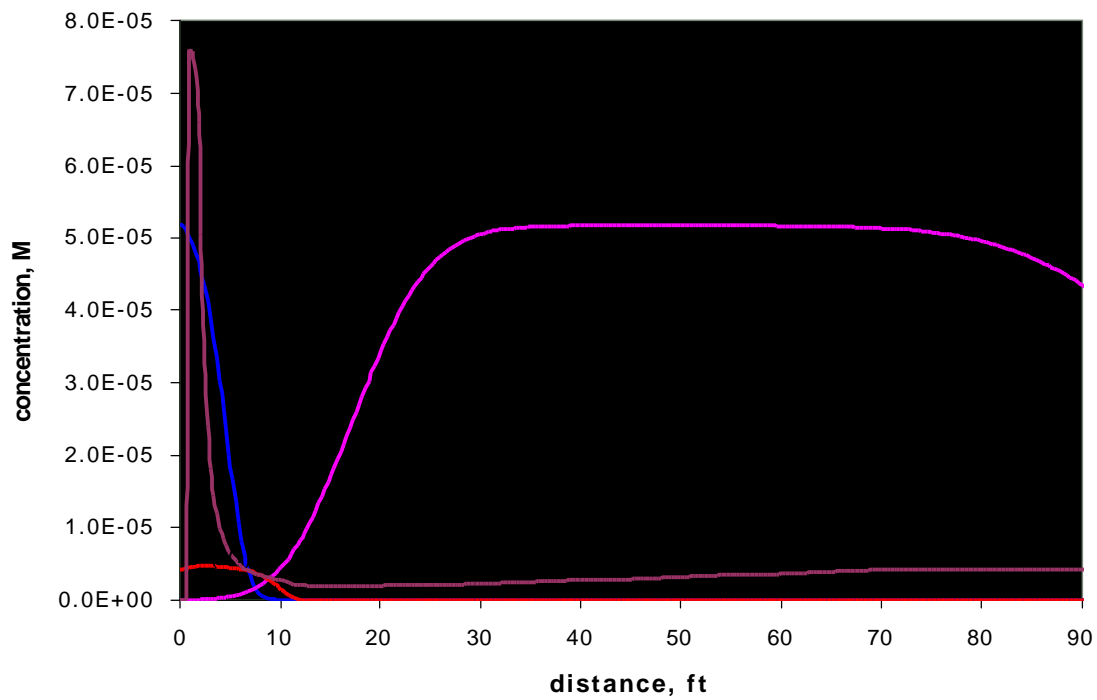


Figure 7. Chemical Concentration Profile after 48 days.

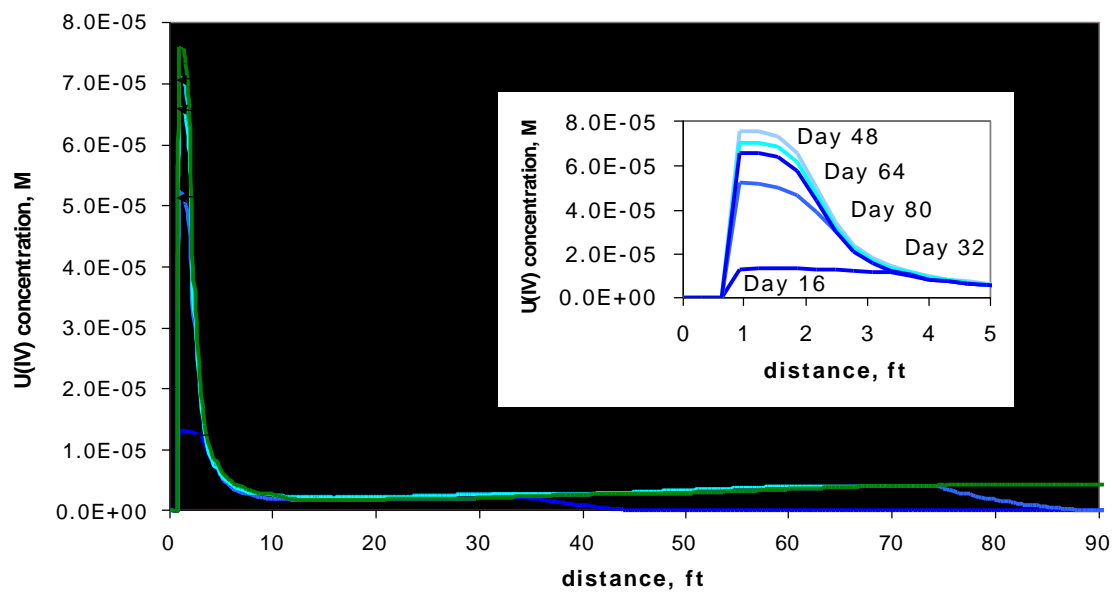


Figure 8. Uranium IV concentration profile over an 80 day period

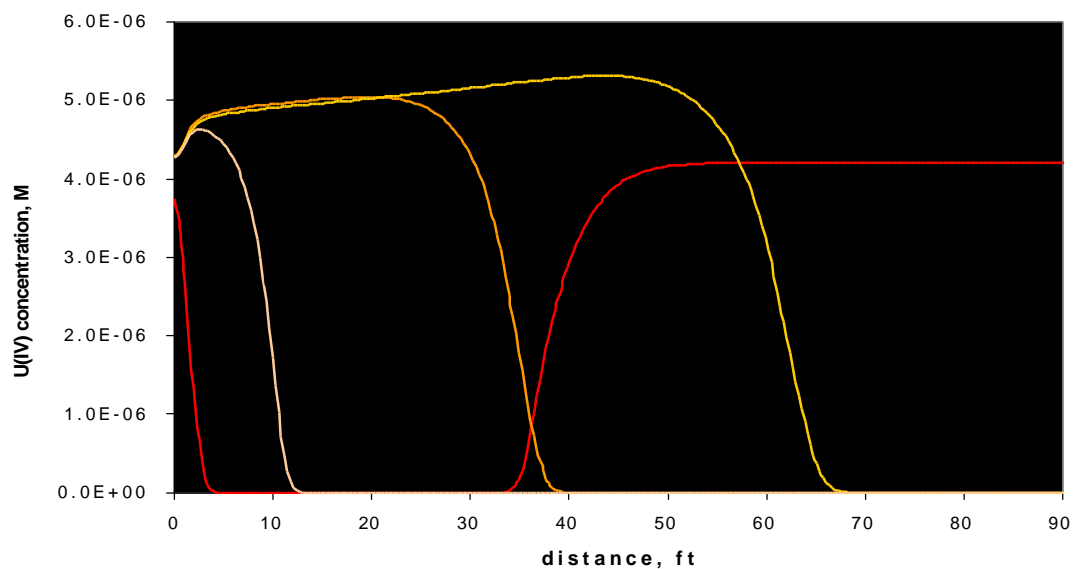


Figure 9. Uranium VI concentration profile over an 80 day period

Preliminary Conclusions from UMTRA Site Uranium Bioremediation Simulations

Although the simulations shown above are very preliminary, and contain only “best guess” kinetic rates, these simulations clearly show the utility of such simulations. They show where bands of U(IV) might precipitate, and can aid experimenters in setting up a monitoring network during demonstration projects. Once properly tested and calibrated, such simulations are extremely helpful for the proper design and operation of a trace metal/radionuclide bioremediation scheme.

IV. REFERENCES

- Alis, O. and Rabitz, H.A., Efficient implementation of high dimensional model representations, to appear in mathematical and statistical methods for sensitivity analysis, edit. by A. Saltelli, John Willy and Sons, 2000.
- Alis, O. and Rabitz, H.A., 1999. General foundations of high dimensional model representations, *J. Math. Chem.*, 25, 197-233.
- Abrams, R.H. and Loague, K., 2000. A compartmentalized solute transport model for redox zones in contaminated aquifers, 2. Field-scale simulations, *Water Resour. Res.*, 36(8), 2015-2029.
- Borden, R.C. and Bedient, P.B., 1986. Transport of dissolved hydrocarbons influenced by oxygen-limited biodegradation; 1. Theoretical development, *Water Resour. Res.*, 22(13), 1973-1982.
- Charlet, L., E. Liger and Gerasimo, P., 1998. Decontamination of TCE- and U-rich waters by granular iron: Role of sorbed Fe(II). *J. Environ. Eng.-ASCE*, 124(1), 25-30.
- Dhakar S.P. and Burdige, D.J., 1996. A coupled, non-linear, steady state model for early diagenetic processes in Pelagic sediments, *Amer. J. Sci.*, 296, 296-330.
- Engesgraad P. and Kipp, K.L., 1992. A geochemical transport model for redox-controlled movement of mineral fronts in groundwater flow systems: A case of nitrate removal by oxidation of pyrite. *Wat. Resour. Res.*, 28(10), 2829-2843.
- Francis, A.J., Dodge, C.J., Lu, F.L., Halada, G.P. and Clayton, C.R., 1994. Xps and xanes studies of uranium reduction by clostridium sp. *Environ. Sci. Technol.*, 28(4), 636-639.
- Grove D.B. and Wood, W.W., 1979. Prediction and field verification of subsurface-water quality changes during artificial recharge, Lubbock, Texas, *Ground Water*, 17(3), 250-257.
- Hunter K.S., Wang, Y. and Van Cappellen, P., 1998. Kinetic modeling of microbially-driven redox chemistry of subsurface environments: coupling transport, microbial metabolism and geochemistry. *J. Hydrol.*, 209, 53-80.
- Jaffé, P.R. and H. Rabitz, H.A., 1988. NABIR Systems Integration Workshop - December 18, 1998 -Summary of Proceedings, Department of Energy, Office of Biological and Environmental Research, Washington, DC.
- Kallin P.L., 1999. Modeling the fate and transport of trace metal contaminants in natural and constructed surface flow wetlands. Ph.D. Dissertation, Princeton University, Princeton, NJ.
- Kindred, J. C., and Celia, M. A., 1989, Contaminant transport and biodegradation; 2, Conceptual model and test simulation, *Water Resour. Res.*, 25, 1149 – 1159.
- Kinzelbach, W., Schäfer, W., and Herzer, J., Numerical modeling of natural and enhanced denitrification processes in aquifers, *Water Resour. Res.*, 27, 1123 – 1135.
- Kirkner, D.J. and Reeves, H., 1988. Multicomponent mass-transport with homogeneous and heterogeneous chemical-reactions - effect of the chemistry on the choice of

- numerical algorithm .1. Theory, *Water Resour. Res.*, 24(10), 1719-1729.
- Lensing H.J., Vogt, M. and Herrling, B., 1994. Modeling of biologically mediated redox processes in the subsurface, *J. of Hydrol.*, 159, 125-143.
- Li, G., Wang, S.W., Rabitz, H.A., Wang, S. and Jaffé, P., Global uncertainty analysis by high dimensional model representations, [*Li et al.*, manuscript in preparation]..
- Lovley, D.R., 1997. Microbial Fe(III) reduction in subsurface environments. *FEMS Microbiol. Rev.*, 20(3-4), 305-313.
- Matsunaga, T., Karametaxas, G., Von Gunten, H.R. and Lichtner, P.C., 1993. Redox chemistry of iron and manganese minerals in river recharged aquifers: A model interpretation of a column experiment. *Geochim. Cosmochim. Acta*, 57, 1691-1704.
- McNab, W.W. and Narasimhan, T.N., 1994. Modeling reactive transport of organic compounds in groundwater using a partial redox disequilibrium approach, *Water Resour. Res.*, 30(9), 2619-1635.
- Miller, C.W. and Benson, L.V., 1983. Simulation of solute transport in a chemical reactive heterogeneous system: model development and application, *Water Resour. Res.*, 19(2), 381-391.
- Molz, F.J., Widdowson, M.A. and Benefield, L.D., 1986. Simulation of microbial growth dynamics coupled to nutrient and oxygen transport in porous media, *Water Resour. Res.*, 22(8), 1207-1216.
- Narasimhan, T.N., White, A.F. and Tokunaga, T., 1986. Groundwater contamination from an inactive uranium tailings pile, *Water Resour. Res.*, 22(13), 1820-1834.
- Park S.S. and Jaffé, P.R., 1996. Development of a redox potential model for the assessment of postdepositional heavy metal mobility, *Ecological Modelling*, 91, 169-181.
- Press, W.H., Teukolsky, S.A., Vetterling, W.T. and Flannery, B.P., 1992. *Numerical Recipes in FORTRAN*, Cambridge University Press, New York, pp. 299-319.
- Rabitz, H.A., Alis, O.F., Shorter, J. and Shim, K., 1999. Efficient input-output model representations, *Computer Physics Communications*, 117, 11-20.
- Rabitz, H.A., Alis, O.F., Shorter, J. and Shim K., Efficient input-output model representations, *Computer Physics Communications*, 117, 11-20, 1999.
- Rabouille, C. and Gaillard, J.-F., 1991. A coupled model representing the deep-sea organic carbon mineralization and oxygen consumption in surficial sediments, *J. Geophys. Res.*, 96, 2761-2776.
- Reeves, H. and Kirkner, D.J., 1998, Multicomponent mass-transport with homogeneous and heterogeneous chemical-reactions - effect of the chemistry on the choice of numerical algorithm .2. Numerical results, *Water Resour. Res.*, 24(10), 1730-1739.

- Salvage, K.M. and Yeh, G.T., 1998. Development and application of a numerical model of kinetic and equilibrium microbiological and geochemical reactions (BIOKEMOD), *J. Hydrol.*, 209(1-4), 27-52.
- Schroth, M.H., Istok J.D., Conner G.T., Hyman M.R., Haggerty R, O'Reilly K.T., 1998. Spatial variability in in-situ aerobic respiration and denitrification rates in a petroleum-contaminated aquifer, *Ground Water*, 36 (6), 924-937.
- Semprini, L., and McCarty, P.L., 1992. Comparison between model simulations and field results for in-situ bioremediation of chlorinated aliphatics, part 2. cometabolic transformations, *Ground Water*, 30(1), 37-44.
- Shim, K., and Rabitz, H.A., 1998. Independent and correlated composition behavior of material properties: Application to energy band gaps for the $Ga_{1-x}In_xP_zAs_{1-z}$ and $Ga_{1-x}In_xP_zSb_zAs_{1-z-y}$ alloys, *Phys. Rev. B.*, 58, 1940-1946.
- Shorter, J. and Rabitz, H.A., 2000. Radiation transport simulation by means of a fully equivalent operational model, *J. Geophys. Res.*, in press..
- Shorter, J., Precila, C. Ip. and Rabitz, H.A., 1999. An efficient chemical kinetics solver using high dimensional model representations, *J. Phys. Chem. A.*, 103(36), 7192-7198.
- Smith, S.L. and Jaffé, P.R., 1998. Modeling the transport and reaction of trace metals in water-saturated soils and sediments. *Water Resour. Res.*, 34(11), 3135-3147.
- Steeffel, C.J. and Lasaga, A.C., 1994. A coupled model for transport of multiple chemical species and kinetic precipitation/dissolution reactions with application to reactive flow in single phase hydrothermal systems, *Am. J. Sci.*, 294, 529-592.
- Sweerts J.R.A., Bar-Gillissen, M-J., Cornelese, A.A. and Cappenberg, T.E., 1991. Oxygen-consuming processes at the profundal and littoral sediment-water interface of a small meso-eutrophic lake (Lake Vechten, the Netherlands), *Limnol. Oceananography*, 36, 1124-1133.
- Tebes-Stevens, C., Valocchi, A., VanBriesen, J.M., and Rittman, B.E., 1998. Multicomponent transport with coupled geochemical and microbiological reactions: model description and example simulations, *J. Hydrol.*, 209, 8-26.
- Truex, M.J., Peyton, B.M., Valentine, N.B. and Gorby, Y.A., 1997. Kinetics of U(VI) reduction by a dissimilatory Fe(III)-reducing bacterium under non-growth conditions. *Biotechnol. Bioeng.*, 55(3), 490-496.
- Tucker, M.D., Barton, L.L. and Thomson, B.M., 1998. Removal of U and Mo from water by immobilized *Desulfovibrio desulfuricans* in column reactors. *Biotechnol. Bioeng.*, 60(1), 88-96.
- Van Cappellen P. and Wang, Y., 1995. Metal cycling in sediments: Modeling the interplay of reaction and transport. In: H.E. Allen (Editor), *Metal Contaminated Aquatic Sediments*, Ann Arbor Press, Ann Arbor, pp. 21-64.
- VanBriesen, J.M. and Rittmann, B.E., 1999. Modeling speciation effects on biodegradation in mixed metal/chelate systems, *Biodegradation*, 10(5), 315-330.

- Wang, S., P.R. Jaffé, G. Li, S.W. Wang, and H.A. Rabitz, 2002. Simulating Bioremediation of Uranium-Contaminated Aquifers; Uncertainty Assessments of Model Parameters. *J. of Contaminant Hydrology*, in press.
- Wang, Y. and van Cappellen, P., 1996. A multicomponent reactive transport model of early diagenesis: Application to redox cycling in coastal marine sediments, *Geochim. Cosmochim. Acta*, 60, 2993-3014.
- Wang, S.W., Levy, II., H., Li, G. and Rabitz, H.A., 1999. Fully equivalent operational models for atmospheric chemical kinetics within global chemistry-transport models, *J. Geophys. Res.*, 104, D23, 30,417-30,426.
- Widdowson, M.A., Molz, F.J. and Benefield, L.D., 1988. A numerical transport model for oxygen- and nitrate-based respiration linked to substrate and nutrient availability in porous media, *Water Resour. Res.*, 24(9), 1553-1565.
- Yeh, G.T. and Tripathi, V.S., 1991. A model for simulating transport of reactive multispecies components: Model development and demonstration, *Water Resour. Res.* 27, 3075-3094.
- Zeh, P., Czerwinski, K.R. and Kim, J.I., 1997. Speciation of uranium in Gorleben Groundwaters, *Radiochimica Acta*, 76, 37-44.